Journal Name

ARTICLE

Alkyloxy modified pyrene fluorophores with tuneable photophysical and crystalline properties

Received 00th January 20xx,
Accepted 00th January 20xx

DOI: 10.1039/x0xx00000x

www.rsc.org/

Andreas Kapf[a], Hassan Eslahi[a,b], Meik Blanke[c], Marco Saccone[c], Michael Giese[c], and Marcel Albrecht*[a]

Novel alkyloxy modified 2,7-di-*tert*-butyl-4,5,9,10-tetra(arylethynyl)pyrenes were prepared through a straightforward SONOGASHIRA coupling approach. Optical properties such as quantum yields and absorption/emission spectra of the fluorophores were investigated by UV/Vis and fluorescence measurements. Aggregation induced excimer formation of the chromophores in polar solvents and in the solid state was proved by the presence of a characteristic bathochromically shifted emission band and a decrease of the emission capability. These results strongly indicate the unexpected observation that the excimer formation of adjacent pyrene rings is not prevented by the introduction of bulky *tert*-butyl substituents. Single-crystal X-ray analysis reveals the co-planar alignment of adjacent molecules and the presence of π-π-stacking in the molecular packing of the pyrene polyaromatics. Furthermore, fluorescence, DSC and POM measurements indicate that the aggregation behaviour, the thermal characteristics and the crystalline properties are significantly influenced by changing structural features of the attached functional groups at the periphery of the pyrene core.

Introduction

Polyaromatic compounds with an expanded π-system have received much attention in various scientific fields such as organic chemistry or materials science as they offer interesting potential applications as electro-phosphorescent emitters,[1] photoluminescent solid state fluorophores,[2] organic field-effect transistors[3] or organic light-emitting diodes (OLEDs).[4–9] Based on their unique optical properties such as high quantum yields and intensive emission bands in the visible range of the spectrum, especially highly conjugated organic compounds are versatile precursors for the construction of novel functional materials. In general, the substitution pattern of fluorophores has a significant effect on the photophysical characteristics of the corresponding organic emitter molecules. Basically, the introduction of bulky substituents at the polyaromatic core effects a perpendicular alignment of each partial structure unit resulting in improved quantum yields and photostability by preventing intermolecular quenching processes. This effect is favourably for potential applications in optoelectronic devices. Taking this into account, various highly branched chromophores with enhanced rigid core structure based on carbazoles,[10–12] triphenylamines,[13] phenoxazines,[14] polyphenylenes,[15,16] tetraphenylethenes[17,18] or fluorenes[19–21] have been developed.

As already mentioned, the presence of bulky substituents prevents the formation of intermolecular π-π-interactions resulting in improved optical properties which are desirable to construct organic emitters. In addition, this effect impedes an efficient molecular packing in the solid or liquid crystalline state, which is essential for various applications based on the transformation between different mesophases. Due to their self-assembly ability especially polyaromatic compounds with an extended π-system have attracted much attention in the synthesis of novel discotic mesogens. In general, this type of substances enables the formation of nematic and columnar mesophases in which adjacent molecules adopt a parallel orientation. This general effect is often connected with a significant shift of the spectral characteristics or enhanced charge transfer properties of the corresponding mesogens. Due to these remarkable features, the structure/alignment relationship of various π-conjugated aromatics have been intensively studied[22–24] resulting in the implementation of new discotic liquid crystals with potential use as OLEDs or semiconducting materials.

Pyrene is an interesting substructure increment for the preparation of fluorescent organic materials as it is easily modified in straightforward synthesis approaches and it exhibit remarkable optical properties such as high quantum yields and improved photo-stabilities.[25,26] Furthermore, pyrene shows a second red-shifted emission band. This process is based on the formation of an excited dimer the so-called excimer complex consisting of an excited fluorophore and a molecule in the ground state. The excimer formation is induced by aggregation resulting in an increased local concentration in the solid state or in solution and this effect is completely reversible upon disassembling of the excimer complex. Due to this remarkable feature, organic pyrene derivatives and polymers have been widely investigated in liquid crystal materials[27–

[a] Institute of Organic Macromolecular Chemistry, Saarland University, Campus C4.2, 66123 Saarbrücken, Germany. E-mail: m.albrecht@mx.uni-saarland.de
[b] Department of Chemistry, College of Science, Shiraz University, Iran
[c] Institute of Organic Chemistry, University Duisburg-Essen, Universitätsstr. 7, 45141 Essen.

Electronic Supplementary Information (ESI) available: [details of any supplementary information available should be included here]. See DOI: 10.1039/x0xx00000x

[30] and in the construction of novel sensor systems for various analytes.[31–35]

As part of our ongoing research of pyrene-modified materials and their application as selective sensors for proteins,[36] we are also investigating the spectral and (liquid) crystalline properties such as quantum yields, excimer emission and phase transition of mesophases of novel 4,5,9,10-tetrasubstituted pyrene derivatives. Especially, the fundamental understanding of the structure-function relationship in the aggregated state is part of our studies as this offers the potential to create materials with tuneable photophysical and mesomorphic behaviour.

Literature known investigations of structural parameters concerning the steric demand of substituents attached to the pyrene core are mainly focussed on 1,6-bi-[37,38] and 1,3,6,8-modified derivatives[39,40] which are readily available by standard synthetic protocols. In general, the introduction of bulky groups prevents the self-assembly of adjacent pyrene molecules resulting in a decreased excimer fluorescence and molecular quenching. This effect was applied in the preparation of various pyrene-based organic emitters exhibiting high quantum yields and aggregation induced emission (AIE) characteristics.[41,42] Increasing the rigidity has the general drawback that efficient packing in the crystalline state is prevented by the perpendicular alignment of the substituents to the pyrene core resulting in the absence of liquid crystallinity of the corresponding compounds. Concepts preparing liquid crystalline pyrene derivatives with concomitant high emission intensity include the introduction of long alkyl chains,[43,44] extending the distance between substituent and core moiety by addition of an acetylene linker,[45–47] the integration of functional groups with secondary binding motifs such as hydrogen bonding[48,49] or applying a 1,3,6,8-substitution pattern.[27] But nevertheless, despite theoretical calculations of the structure/alignment relationship and its effect on the solid state and spectral characteristics, inducing liquid crystallinity of modified pyrenes is based on empirical studies[50] and often results in compounds showing undesired molecular quenching upon aggregation processes at high concentrations or in the solid state. Based on these considerations, the development of novel organic emitters exhibiting tuneable optical and crystalline properties is an important research field with great impacts on the construction of opto-electronical devices and/or sensor systems. Literature known approaches of the analysis of the optical and electrochemical properties of arylethynyl pyrenes are mainly focussed on the 1,3,6,8-[51–55] and 2,7-substitution pattern[56,57] as the corresponding starting materials are readily available. In addition, systematic investigations of donor modified *N*,*N*-(dimethyl anilineethynyl) pyrenes were performed by Kim and co-workers.[51] Depending on the substitution pattern and the donor capability of the attached substituents photophysical and electrochemical characteristics such as electrogenerated chemiluminescence (ECL) can be efficiently tuned resulting in novel emitter moleculeswhich are applicable as OLED materials. Furthermore, Kato and co-workers investigated the aggregation behaviour and the photophysical properties of various arylethynyl pyrenes with different substitution pattern.[58] Due to enhanced π-π-interactions between the expanded aromatic framework of adjacent molecules, especially 2,4,5,7,9,10-hexaethynyl pyrenes show a high self-assembly efficiency resulting in a characteristic phase transition from the crystalline to the liquid crystalline state. But to the best of our knowledge, systematic investigations of hydrophobic effects on the aggregation and optical characteristics of ethynyl modified pyrenes have never evaluated before.

Herein, we report a straightforward synthesis approach of novel 4,5,9,10-tetrasubstituted pyrene derivatives bearing phenyl acetylene linker and alkyl ether functionalities with variable chain lengths (Scheme 1).

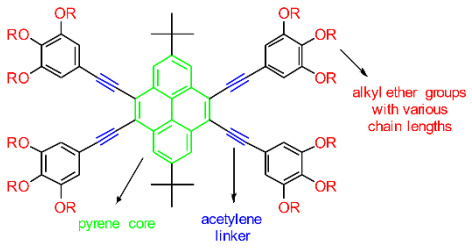

Scheme 1. Structures of the 4,5,9,10-tetrasubstituted pyrenes.

The materials design concept of the resulting products is based on the pyrene core structure exhibiting desired photophysical properties such as high quantum yields. Introduction of acetylene linker units effects both a co-planar alignment of the phenyl substituents and a bathochromic shift of the emission maximum by extending the conjugation length of the fluorophores. Furthermore, variation of the substitution pattern of the alkyl ether functionalities at the phenyl rings and extension of the chain lengths offers the potential to create chromophores with tuneable self-assembly and liquid crystalline characteristics which can be monitored by the excimer formation in solution or in the solid state. Variation of structural features such as the extension the chain length of the alkyl ether groups will have a significant impact of the hydrophobicity and self-assembly capability of the resulting fluorophores. Especially, changes of the solvent polarity have a significant impact on the local concentration of the investigated emitter molecules which can be detected by optical changes of the emission wavelength and quantum efficiency. This general effect is essential to create lyotropic OLED materials or sensors which are sensitive to variations of the local hydrophobicity of the analyte/sensor aggregate.

Photophysical properties such as fluorescence emission bands and quantum yields were analysed in different solvents and in the solid state. The presence of a characteristic bathochromic shift of the emission maximum from blue to yellow-green indicates the formation of excimers which were caused by molecular self-assembly and aggregation processes. Surprisingly, the generation of excimers was not inhibited by attaching bulky *tert*-butyl groups to 2- and 7-positions of the pyrene core. To get deep insight on the structure-property relationship which drive the assembly of our pyrene fluorophores in the solid state, we performed an in deep packing analysis, where single crystal X-ray diffraction is complemented by quantum chemical calculations and Hirshfeld surface analysis. Furthermore, to the thermal behaviour of the pyrene derivatives has been analysed by polarized optical microscopy (POM) and differential scanning calorimetry (DSC) exhibiting a discotic nematic phase for one derivative.

Experimental Section

Materials

Solvents were purified according to standard procedures. Water was deionized and further purified with a Milli-Q water purification system (ELGA PURELAB *Classic* UFV). 5-Bromophenyl-1,2,3-triol and 2,7-di-*tert*-butylpyrene were prepared according to literature known procedures.[59,60] Unless otherwise specified, all chemicals were purchased from commercial sources and were used as received: 5-bromo-1,2,3-trimethoxybenzene (TCI Europe), 4-bromophenol (TCI Europe), 1-bromobutane (Sigma Aldrich), 1-bromohexane (Sigma Aldrich), 1-bromooctane (TCI Europe), 1-bromodecane (TCI Europe), copper(I) iodide (Riedel-de Haën), $Pd(PPh_3)_2Cl_2$ (Carbolution), TMSA (TCI Europe), triphenylphoshine (Sigma Aldrich), potassium fluoride dihydrate (Sigma Aldrich), pyrene (Sigma Aldrich).

Instruments and theoretical methods

NMR spectra were recorded on a Bruker Avance Ultrashield 400 spectrometer (400.2 MHz for proton and 100 MHz for carbon measurements) at room temperature. Absorption spectra were recorded using an Evolution 220 UV/Vis spectrophotometer (Thermo Scientific), and emission spectra with a commercial Jasco spectrofluorometer (Jasco, FP-6500). All spectra were recorded in quartz cuvettes (3 mL content, 1 cm layer thickness, Hellma Analytics 117.11-FQS) and samples were degassed by bubbling nitrogen through the corresponding solutions for 15 min. Solid samples were measured at quartz plates (Hellma Analytics 363-QC). Thin films were prepared by slow evaporation of a diluted THF solution of the corresponding compound. Crystal structures were measured using a X8, Apex II X-ray diffractometer. Polarized optical microscopy (POM) images were taken on a Nikon Eclipse Ni microscope with crossed polarizers equipped with a Linkam hot stage. The images were recorded by an Imaging Source camera (DFK23UX174). DSC thermograms were received using a DSC 3+ from Mettler Toledo with a heating/cooling speed of 10°C/min (sample weight ~3 mg) in an argon atmosphere. MALDI measurements were performed using a Bruker, Autoflex Speed MALDI-TOF-TOF-spectrometer in positive reflector mode (High Resolution from 200-5000 Da with MTP 384 Big Anchor 800 as a target and dithranol as a matrix. Calculations were performed on a pc equipped with an Intel® Core™ i5-7400 Processor and 8 GB RAM and the *CrystalExplorer* program. The model energies were calculated using the option "*accurate*". A cluster of molecules within a radius of 3.8 Å from the reference molecule was considered.

See http://130.95.176.70/wiki/index.php/Intermolecular_Interaction_Energies for further details. Molecular electrostatic potentials mapped on the Hirshfeld surfaces were also generated with *CrystalExplorer*.

Results and discussion

Synthesis and characterisation of the 4,5,9,10-tetrasubstituted pyrene derivatives

The 4,5,9,10-tetra(arylethynyl)pyrenes **6a-h** were synthesized through a SONOGASHIRA coupling starting from 2,7-di-*tert*-butyl-4,5,9,10-tetrabromopyrene[61] (**5**) and the corresponding trialkoxy- (**4a-d**) and monoalkoxy phenylacetylenes (**4e-h**) in the presence of catalytic amounts of $Pd(PPh_3)_2Cl_2$, CuI and triphenylphosphine (Scheme 2).

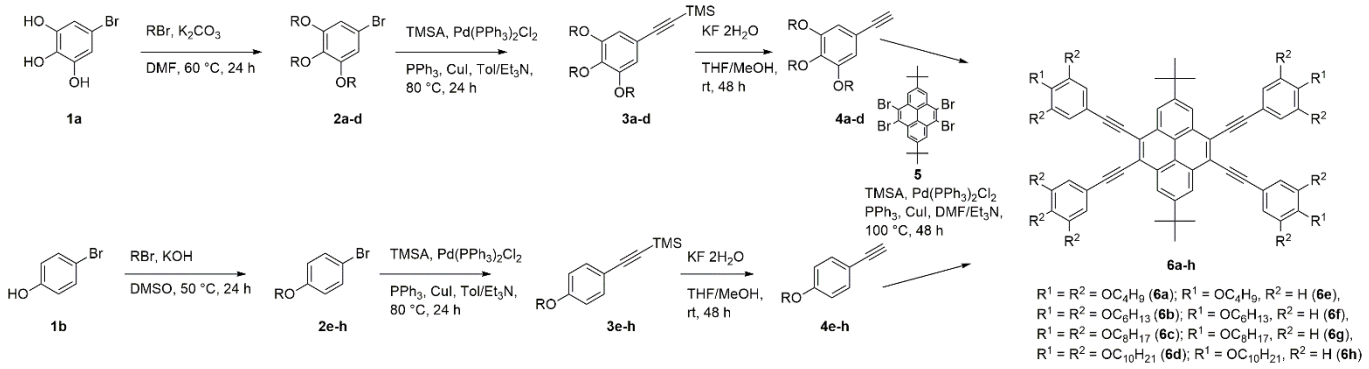

Scheme 2. Synthesis of the 4,5,9,10-tetrasubstituted pyrenes **6a-h**.

Tri-substituted phenyl acetylenes **4a-d** were prepared by alkylation reaction of 5-bromophenyl-1,2,3-triol **1a** with the corresponding 1-bromoalkanes, subsequent SONOGASHIRA coupling with trimethylsilylacetylene (TMSA), followed by deprotection with potassium fluoride in overall moderate yields over three steps. A similar synthetic approach was applied for the corresponding monoalkoxy derivatives (**4e-h**) except that commercially available 4-bromophenol **1b** was used as starting material. The 4,5,9,10-tetrasubstituted pyrenes **6a-h** were obtained as light-yellow solids and were fully characterized by common analytical techniques such as ^{1}HNMR, ^{13}CNMR and high-resolution mass spectroscopy (HRMS). All compounds are soluble in common organic solvents such as cyclohexane, toluene, dichloromethane or THF. Due to the hydrophobicity of the polyaromatic framework and the presence of long alkyl chains, the solubility of the 4,5,9,10-tetrasubstituted pyrene derivatives in more polar solvents such as ethanol, DMF or

acetonitrile is gradually decreased indicated by the formation of turbid suspensions.

Description of the crystal structures and Hirshfeld surface analysis

Single crystals of **6e** and **6h** were obtained by slow evaporation of a CH_2Cl_2/EtOH mixture (10:1, v/v). The crystallographic data of the corresponding pyrene derivatives are presented in the Supporting Information. **6e** displays a C_{2h} symmetric structure with a two-fold axis (Figure 1). The four phenyl rings are slightly twisted with angles of 5.0° for the C(27)-C(32) ring and 6.2° for the C(15)-C(20) ring relative to the pyrene core, respectively. In addition the acetylene carbon atoms are slightly distorted with twist angles of 11.6° for the C(13)-C(14) bond and 4.5° for the C(25)-C(26) bond, respectively. The
alkoxy groups are nearly co-planar relative to their corresponding phenyl rings with twist angles of 2.8° (O(1)) and 0.5° (O(2)).

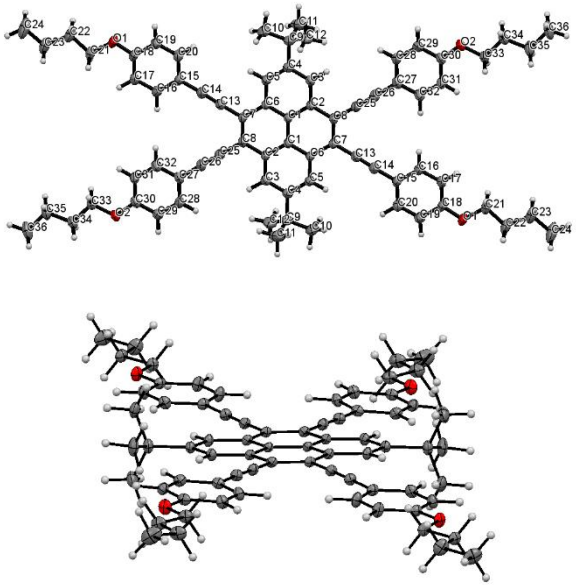

Figure 1. X-ray single structure of **6e** (*top*) top view and (*bottom*) side view.

The crystal packing of **6e** shows a layer-type alignment of adjacent molecules with an interplanar distance of about 3.5 Å (Figure 2). Pyrene rings of adjacent molecules exhibit a co-planar arrangement. π-π-stacking interactions between the C(15)-C(20) phenyl rings of any individual polyaromatic system with one pyrene core of each layer were observed in an average distance of 3.6 Å. This intermolecular π-π-stacking was located between pyrene rings of the non-K-region and the adjacent phenyl rings of the substituted acetylene groups. Due to this observation, the presence of bulky *tert*-butyl groups at the pyrene core is not preventing the formation of hydrophobic π-π-interactions. Interestingly, compared to previous results of Yamato and co-workers which investigate molecular structures of mono- and 2,7-di-*tert*-butyl-substituted pyrene derivatives,[62,63] the remaining C(27)-C(32) phenyl rings as well as adjacent pyrene moieties show no π-π-stacking indicating the steric demands of the long alkyl chains which prevent a dense molecular packing of the complete system.

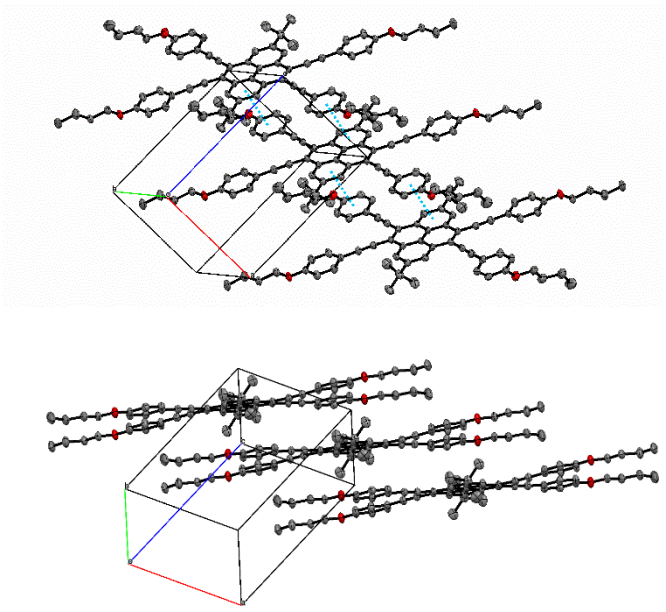

Figure 2. Crystallographic packing of **6e**. (*top*) π-π-Stacking interactions of adjacent molecules are highlighted in blue colour. (*bottom*) Side view of the layer-like structure of **6e**. Hydrogen atoms are omitted for clarity.

In addition, various intermolecular contacts below the sum of the van der Waals radii of the respective atoms could be observed in the molecular packing of pyrene **6e** (Figure 9, Supporting Information). These interactions include multiple C-H···π interactions between hydrogen atoms of the *n*-butyl chain of the alkyl ether moiety and carbon atoms of the acetylene functionality (H21···C26) and the aromatic phenolic benzene rings (H16···C29), respectively. These results indicate that the presence of the alkyl ether chains at the periphery of the pyrene core is essential obtaining a dense molecular packing. Similar results with a co-planar orientation of both the pyrene and the phenyl substituents were obtained for compound **6h**, except that no π-π-stacking between individual molecules was observed. Furthermore, in addition to C-H···π interactions between alkyl groups of the phenyl ether moiety and aromatic atoms of the pyrene or phenolic benzene rings additional CH···CH interactions between hydrogen atoms of adjacent alkyl chains and/or aromatic ring hydrogens are present in the packing diagram of *n*-decyl derivative **6h** (Figure 12, Supporting Information). The increased overall number of intermolecular interactions compared to the corresponding *n*-butyl pyrene demonstrate the general impact of the chain length of the hydrophobic groups on the molecular packing in the solid state. Crystallographic parameters such as twist angles and molecular packing are provided in the Supporting Information section.

The Hirshfeld surface of **6e** was mapped over the shape index and the most significant interactions *i.e.* H···H, C···H/H···C and C···C were quantitatively analyzed. In Figure XX the two dimensional fingerprint plots are shown which demonstrate the difference between the intermolecular interaction patterns and the relative contributions (in percentage) for the significant intermolecular interactions associated with the molecule. Intermolecular interactions become visible as distinct spikes in two dimensional fingerprint plots. Complementary regions are observable in

fingerprint plots where one molecule acts as a donor ($d_e > d_i$) and the other as an acceptor ($d_e < d_i$).

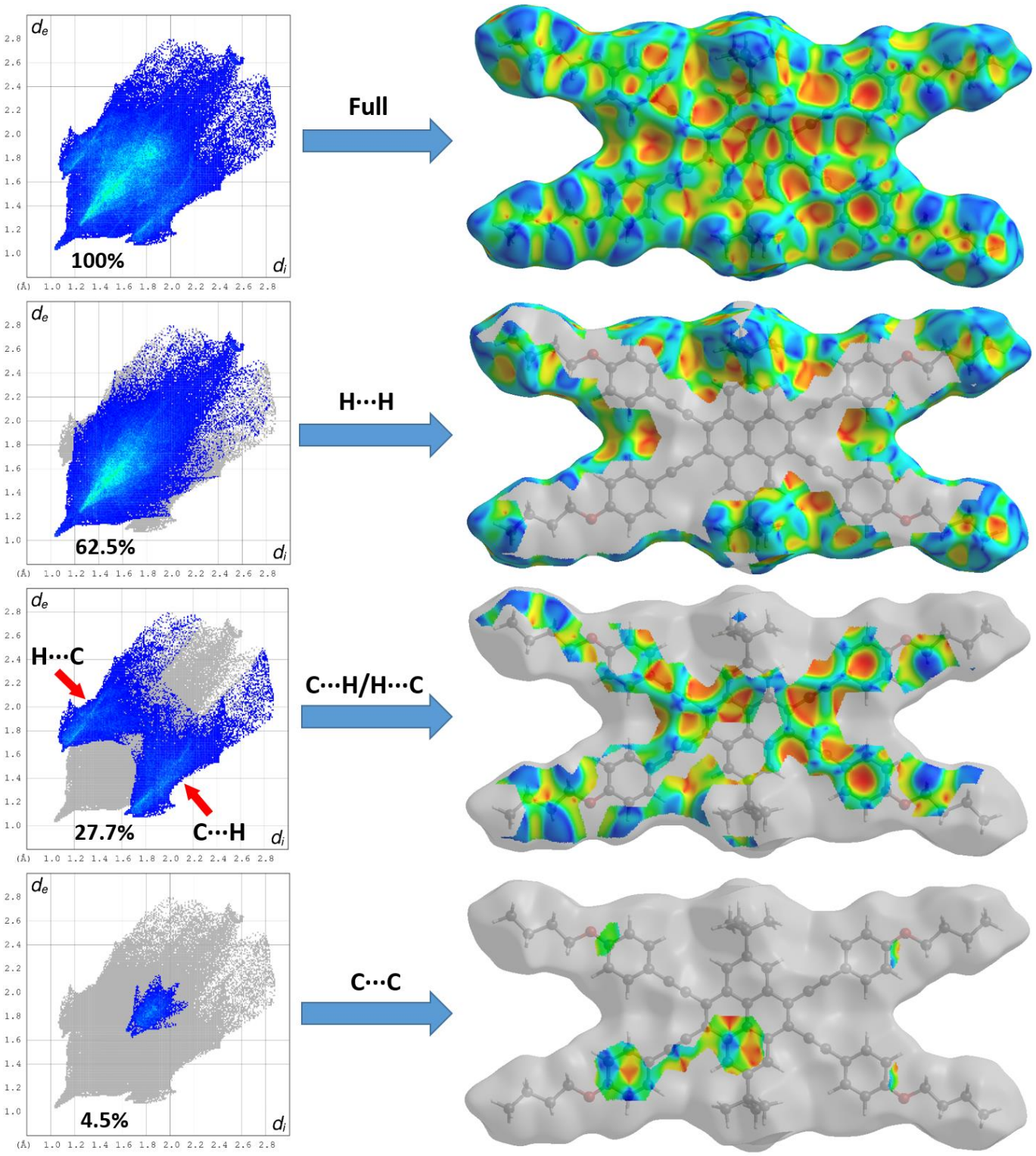

Figure 3. Fingerprint plots of **6e**: full and resolved into different interactions showing the percentages of contacts contributing to the total Hirshfeld surface area of the molecule. Surfaces in the right hand columns highlight the relevant surface patches associated with the specific contacts in the total Hirshfeld surface area of **6e**.

Theoretical insights

In order to give a rigorous energetic quantification to the non-covalent interactions which showed up in the fingerprint plots of Figure XX, we performed a computational analysis of the crystal structure of **6e**. We thus selected a reference molecule in the crystalline packing (as provided by *CrystalExplorer*) and then molecule pairs formed by the reference molecule with surrounding molecules were analysed with respect to their intermolecular

interactions. For our analysis we selected the six most significant pairs from the point of view of the interaction energy. These pairs are called structure determinants, and are identified by several quantities which are Explained in detail in the ESI and provided in Figure AA ESI. A special bonus of the *CrystalExplorer* suite of programs is that it provides an effective energy decomposition scheme, which allow one to decompose the interaction energy into physically sound contributions such as electrostatics, dispersion, polarization and repulsion. Figure XY summarizes our findings: the Structure Determinant which gives a dominating contribution to the crystal packing (147.5 kJ/mol) feature multiple slipped stacked (or displaced) π···π interactions. This interaction is dominated by a significant dispersive contribution of 225 kJ/mol while the electrostatic contribution is less than 10% of this value (Figure AA ESI). The next two Structure Determinants in our ranking feature several CH_{aliph}···π interactions already mentioned above and the last two are weakly bound by van der Waals forces which are dispersive in nature (Figure AA ESI).

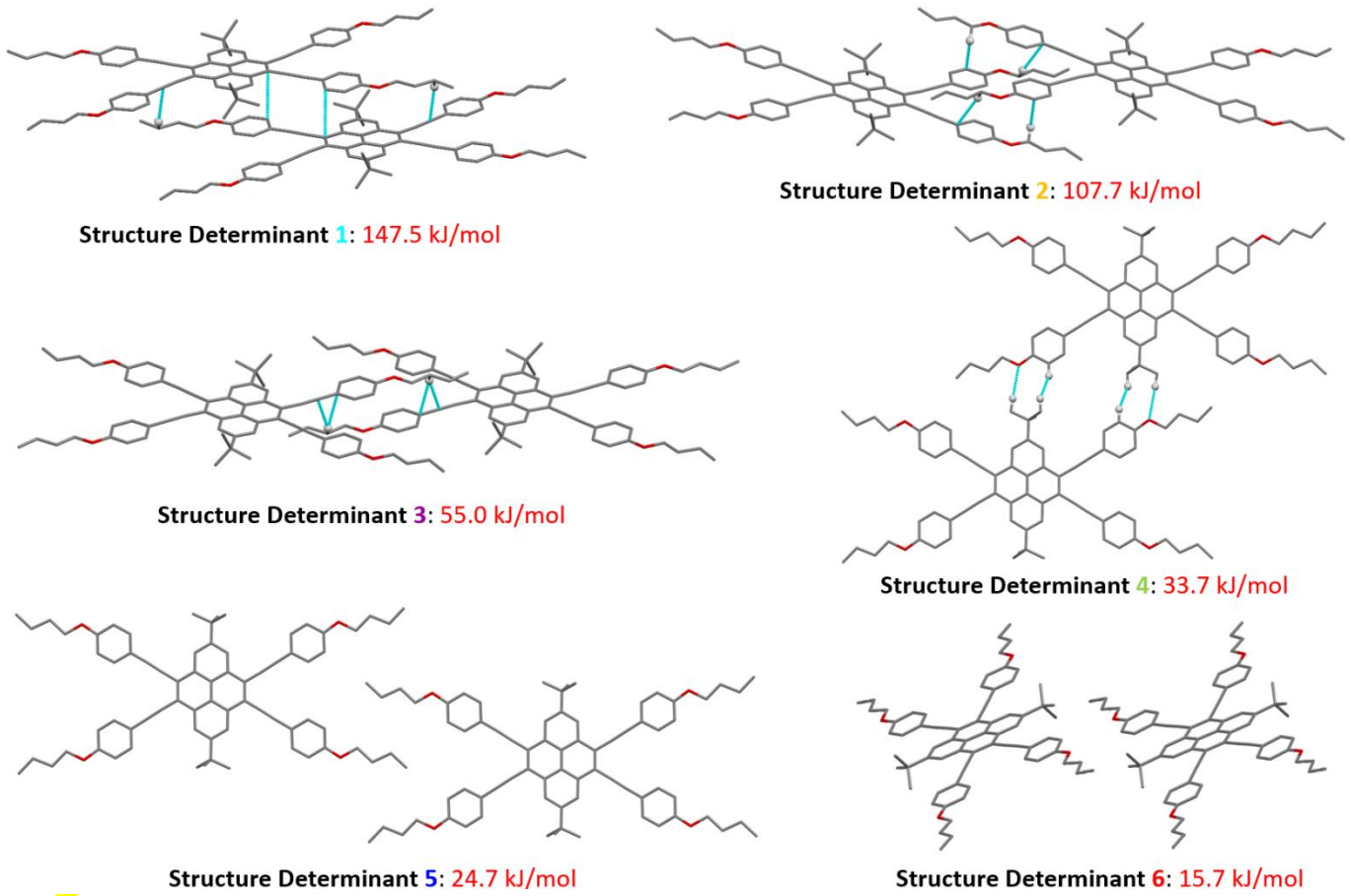

Figure XY. Capped stick representation of the six most stabilizing interactions in the **6e** structure as provided by CrystalExplorer. Blue lines represent short intermolecular contacts below the sum of the van der Waals radii of the respective atoms. Hydrogen atoms involved in short contact interactions are represented as isotropic spheres. Color chart: grey = C, white = H, red = O, purple = N, yellow = S. For the color codes corresponding to each Structure determinant see ESI.

Photophysical properties

As already mentioned, the substitution pattern of the pyrene derivatives has an direct impact on their self-assembly behaviour and thus on their photophysical properties in solution and in the solid state. Therefore, we analysed the specific aggregation behaviour of polyaromatics 6a-h **by monitoring optical features, such as position of the emission maximum, size of the quantum yields and appearance of a characteristic excimer emission. Spectroscopic characteristics such as absorption maximum appearing at the longest wavelength, emission maximum and quantum yields were analysed by UV/Vis and fluorescence measurements of highly diluted solutions of compounds** 6a-h **in dichloromethane (Table 1).**

Table 1 Optical spectroscopic data for the substituted pyrenes **6a-h**.

	λ_{abs} [a] [nm]	λ_{em} [b] [nm]	Stokes shift [cm^{-1}]	Φ_f [c]
6a	417	469	2659	0.63
6b	417	471	2749	0.63
6c	417	469	2659	0.62
6d	417	469	2659	0.66
6e	417	452	1857	0.73
6f	417	453	1906	0.65
6g	417	453	1906	0.64
6h	417	452	1857	0.60
Di-*tert*-butylpyrene	377	379	140	0.03

[a]Longest absorption wavelength measured in dichloromethane at a pyrene concentration of ~10^{-5} M. [b]Emission bands measured in dichloromethane at a pyrene concentration of ~10^{-5} M. [c] Absolute quantum yields in dichloromethane (~10^{-5} M).

All compounds show intensive absorption bands at 300-350 nm and an additional maximum at 417 nm (Diagram 1).

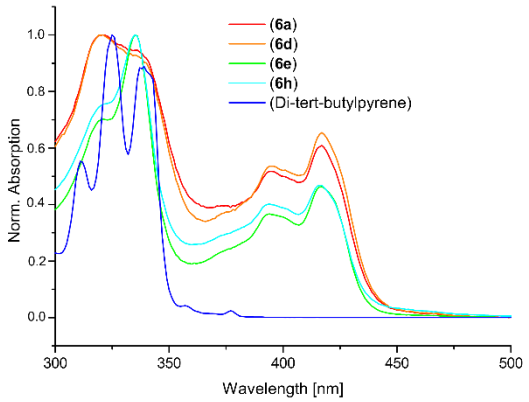

Diagram 1. Normalized absorption spectra of substituted pyrene derivatives **6a/d**, **6e/h** and di-*tert*-butyl pyrene. Spectra were recorded in dichloromethane at a concentration of 10^{-5} M.

Compared to the unsubstituted 2,7-di-*tert*-butyl pyrene, which exhibit absorption bands exclusively in the UV region, the presence of this characteristic band at 417 nm indicates the expanded conjugation of the pyrene chromophores with the four substituted acetylene groups in 4-, 5-, 9-, and 10-positions. The investigated absorption band of **6a-h** are in accordance to the corresponding monomethoxy functionalized pyrene derivative analysed by Yamato and co-workers which shows a characteristic absorption maximum at 415 nm.[62]

Interestingly, absorption bands between 380 nm and 450 nm are almost identical for the tri- (**6a-d**) and monoalkoxy functionalized pyrene derivatives (**6e-h**), whereas the two general substitution patterns slightly differ in their maximum absorption band in the UV region. Compounds **6a-d** show a hypsochromic shifted band at 321 nm compared to the mono functionalized derivatives (**6e-h**), which exhibit an absorption maximum at 335 nm indicating an enhanced electron-donating effect of the three alkoxy groups attached at each phenyl substituent.

Excitation of diluted solutions of compounds **6a-h** at 340 nm resulted in an intensive emission in the blue region between 452-471 nm (Diagram 2). Emission spectra are independent of the excitation wavelength and concentration of the corresponding fluorophore indicating the absence of any self-aggregation processes in dichloromethane in the investigated concentration range of 10^{-5}-10^{-2} M. Normalized emission spectra of the tri-modified chromophores **6a-d** are almost identical with maxima at about 470 nm whereas the monoalkoxy functionalized pyrene derivatives **6e-h** show an intensive emission at about 450 nm. This bathochromic shift of about 20 nm can be explained by an enhanced electron-donating effect of the three alkoxy groups resulting in a decrease of the energy gap between the ground and the excited state compared to the mono functionalized derivatives **6e-h**. Similar results were obtained the corresponding monomethoxy functionalized pyrene derivative published by Yamato and co-workers which exhibit a characteristics emission band at 453 nm.[62] This value is in accordance to monoalkoxy functionalized derivatives **6e-h** which show emission maxima at 452 and 453 nm. Furthermore, absolute quantum yields of the prepared fluorophores are in the range of 0.60-0.73 indicating that excitons are completely confined to the entire polyaromatic system, due to the expanded conjugation between the pyrene core and the four aromatic acetylene substituents. The measured quantum yields are similar to the ones of the corresponding 2,7-di-*tert*-butyl-4,5,9,10-tetra(arylethynyl)pyrenes investigated by Yamato and co-workers which are in the range of 0.66-0.98.[62] These results indicate the structural relationship between pyrene chomophores **6a-h** and the previous reported ones.

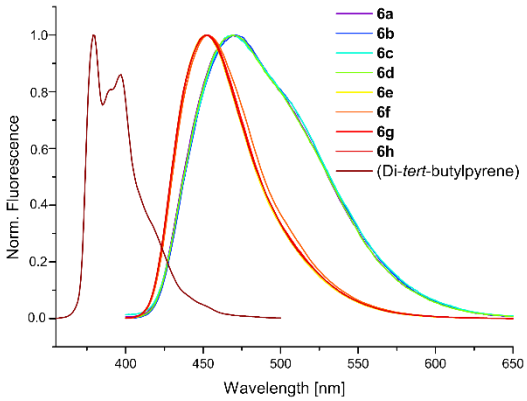

Diagram 2. Normalized emission spectra of substituted pyrenes **6a-h** and di-*tert*-butyl pyrene. Spectra were recorded in dichloromethane at a concentration of 10^{-5} M.

The aggregation of the 4,5,9,10-tetra(arylethynyl)pyrenes **6a-h** was investigated by UV/Vis and fluorescence measurements in different solvents and in the solid state. Compared to diluted solutions in non-polar solvents such as dichloromethane or toluene absorption spectra of the corresponding pyrene derivatives show a complete loss of the vibronic characteristics in thin films and polar solvents such as acetonitrile or DMF (Diagram 3, exemplarily shown for **6c**). This observation is a result of self-aggregation processes in the solid state and polar solvents yielding to a quenching of the fluorescence. Nevertheless, no significant shift of the characteristic absorption bands at 394 and 416 nm can be observed.

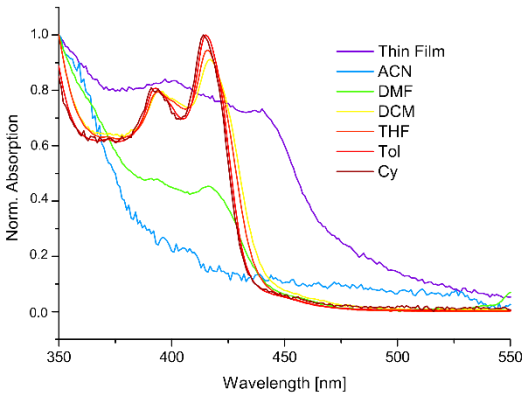

Diagram 3. Normalized absorption spectra of substituted pyrene derivative **6c** in different solvents and as a thin film. Spectra were recorded at a concentration of 10^{-5} M for non-polar solvents such as cyclohexane (Cy),

toluene, THF or DCM and in saturated solutions of polar solvents such as DMF or acetonitrile (ACN).

Compared to the fluorescence spectrum in dichloromethane thin films of chromophores **6a-h** are bathochromically shifted with values of around 57 nm due to self-aggregation (Diagram 4). This colour change in the emission maximum from blue to green/yellow is characteristic for the excimer formation of pyrene derivatives. Based on these results excimer formation is not prevented by the presence of bulky substituents such as the *tert*-butyl groups at 2- and 7-position of the pyrene core which is in contrast to the observation that excimer formation is excluded for 3,8-di-tert-butylpyrene published by Castellano *et al.*[64] Interestingly, the bathochromic shift is increased after annealing thin films of **6c** for 1 h at 100 °C indicating that the structural alignment of individual chromophores was optimized at higher temperatures forming a densely packed solid phase with enhanced excimer emission.

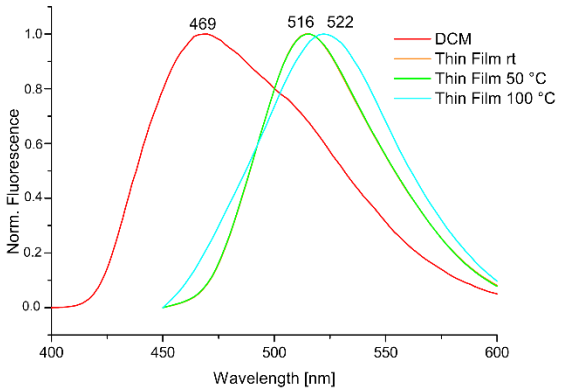

Diagram 4. Normalized fluorescence spectra of substituted pyrene derivative **6c** in dichloromethane (10^{-5} M) and as a thin film at different temperatures and an excitation wavelength of 340 and 410 nm, respectively. Thin films of **6c** were annealed at the specified temperature for 1 h. Thin film emission curve at room temperature is congruent with the one measured at 50 °C.

Furthermore, self-aggregation and solvatochromic effects of the prepared pyrene compounds in solvents with different polarity were investigated by analysing the position of the emission maximum and quantification of the quantum yields. The results are presented in table 2. In general, increasing the polarity of the solvent results in a significant bathochromic shift of the emission wavelength of polyaromatics **6a-h** (Diagram 5 and Supporting Information) which can be attributed to changes of the quadrupole moments of the ground and excited state in different solvents and/or the aggregation induced excimer formation. In particular, solvatochromic effects can be assumed for highly diluted solutions of **6a-h** in non-polar solvents providing an increased solubility of the polyaromatics without the probable formation of excimers. In polar solvents such as DMF or acetonitrile bathochromic shift are basically induced by aggregation processes resulting in a maximum emission band close to the characteristic excimer fluorescence of pyrene. For example, the emission maximum of pyrene **6a** in cyclohexane is localized at 433 nm whereas a bathochromic shift of 100 nm was observed upon changing to DMF.

Table 2 Emission characteristics of the substituted pyrenes **6a-h**.

		6a	**6b**	**6c**	**6d**	**6e**	**6f**	**6g**	**6h**
solid	Φ_f [a]	0.29	0.38	0.32	0.38	0.28	0.23	0.12	0.12
Cy	λ_{em} [b] [nm]	433	433	433	433	426	427	426	429
	Φ_f [a]	0.52	0.53	0.49	0.53	0.50	0.43	0.68	0.33
Tol	λ_{em} [b] [nm]	439	439	439	439	432	432	432	432
	Φ_f [a]	0.58	0.60	0.55	0.61	0.62	0.56	0.57	0.51
THF	λ_{em} [b] [nm]	461	459	462	459	439	439	439	439
	Φ_f [a]	0.59	0.58	0.56	0.59	0.62	0.59	0.59	0.54
DCM	λ_{em} [b] [nm]	469	471	469	469	452	453	453	452
	Φ_f [a]	0.63	0.63	0.62	0.66	0.73	0.64	0.65	0.60
DMF	λ_{em} [b] [nm]	533	532	521	518	462	468	464	463
	Φ_f [a]	0.26	0.29	0.23	0.06	0.50	0.54	0.68	0.56
ACN	λ_{em} [b] [nm]	525	519	520	514	472	464	467	460
	Φ_f [a]	0.20	0.15	0.09	0.02	0.42	0.42	0.42	0.12

[a]Absolute fluorescence quantum yield measured in the solid state or in solution (~10^{-5} M) at an excitation wavelength of 340 nm. [b]Longest emission wavelength measured at a pyrene concentration of ~10^{-5} M and an excitation wavelength of 340 nm

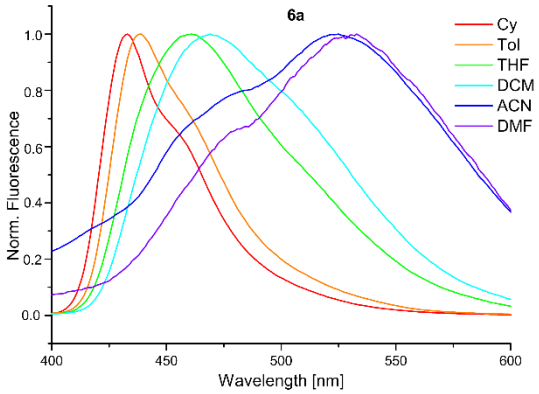

Diagram 5. Normalized fluorescence spectra of substituted pyrene derivative **6a** in different solvents at a concentration of 10^{-5} M excited at a wavelength of 340 nm.

Similar results were obtained for all tri-alkoxy modified pyrene derivatives **6a-d**. In contrast, the solvatochromic shifts of the emission wavelength of the mono-substituted chromophores **6e-h** are smaller (30-40 nm). This significant difference can be explained by increased hydrophobic interactions of the three alkyl chains attached at each phenyl group of the pyrene core resulting in a decreased solubility in polar solvents and a higher concentration of polyaromatic π-aggregates which enables a closer molecular packing between adjacent pyrene fluorophores. Based on this observation molecular self-assembly and excimer formation in polar solvents is directly affected by the hydrophobicity of the four substituents attached at the pyrene backbone. Compared to previous results of Yamato and co-workers, which emphasized the inhibition of π-π-interactions between adjacent pyrene moieties by the presence of the bulky *tert*-butyl groups,[62,63] the present work on the photophysical properties of the hydrophopic pyrene chromophores strongly indicates the formation of close aggregates emitting a characteristic excimer fluorescence. Furthermore, aggregation induced excimer formation can be analysed by estimating the absolute fluorescence quantum yields in various solvents and in the solid state. In non-polar solvents such as cyclohexane, toluene, THF and DCM pyrenes **6a-h** show quantum yields in a range 0.43-0.73 revealing the presence of isolated chromophores which exhibit no significant self-quenching processes. Due to self-aggregation in the solid state and in polar solvents such as DMF and acetonitrile quantum yields remarkably decrease reaching values from 0.02 to 0.42 which is characteristic for quenching effects of substituted pyrene derivatives induced by the excimer.[65] Furthermore, quantum yield changes of the tri substituted pyrenes (**6a-d**) differ from the one obtained from the mono alkoxy (**6e-h**) modified pyrene derivatives. By changing the solvent from DCM to acetonitrile quantum yields of **6a-d** decrease from 0.62-0.66 to 0.02-0.20 whereas the overall quantum yield change of the mono-alkoxy modified chromophores is significantly smaller with values of about 0.20. Interestingly, as an exception mono-substituted *n*-decyl derivative **6h** shows similar results compared to tri alkylated ones. These observations indicate that hydrophobicity of the corresponding fluorophores is strongly related to structural parameters such as alkyl chain length and number of the alkoxy groups attached to the phenyl rings resulting in different aggregation and photophysical characteristics. Solvatochromic shifts of the emission maximum and quantum yield changes imply that aggregation and excimer formation is favoured by the presence of an increased number of hydrophobic phenyl rings bearing long alkyl chains. In addition, quantum yields in the crystalline state of compounds **6e** and **6h** with values of 0.24 and 0.13 are almost identical with the ones measured in the amorphous state. These results indicate quenching processes are independent from the composition of crystalline parameters in the solid state.

To get further insights into the relationship between hydrophobicity and aggregation characteristics the corresponding substituted pyrenes fluorescence emission spectra of **6a** and **6d** were recorded in various THF/water ratios (Diagram 6).

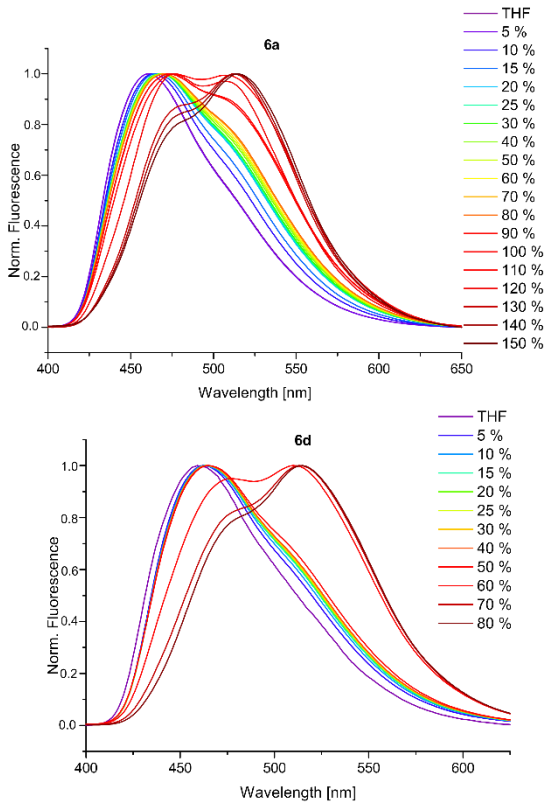

Diagram 6. Normalized fluorescence spectra of substituted pyrene derivative **6a** (*top*) and **6d** (*bottom*) in different THF/water mixture ratios. Measurements ´were performed at a concentration of 10^{-5} M and an excitation wavelength of 340 nm.

In general, increasing the polarity of the solvent by addition of water results in the stepwise appearance of a characteristic excimer emission band at 515 nm. Due to the increased hydrophobicity of the tri substituted *n*-decyl derivative **6d** compared to the corresponding *n*-butyl compound **6a**, a significant excimer band was observed at THF/water ratios above a water content of 60 %. In contrast to that excimer formation of pyrene **6a** was induced at much higher water contents of about 120 % indicating tuneable aggregation characteristics of the investigated polyaromatics by changing structural features of the attached functional groups at the periphery of the pyrene core.

Thermal behaviour

Thermal properties of the resulting products **6a-h** were analysed by differential scanning calorimetry. Melting points of all tetrasubstituted pyrenes are in the range of 79-330 °C determined by calculating the arithmetic average of the maximum endothermic peak of three melting/cooling cycles (Supporting Information). In general, increasing the number of alkoxy groups at the phenyl rings attached to the pyrene core or extending the length of the alkyl chains result in a decrease of the corresponding melting points. For example, the melting points of the 4,5,9,10-tetrasubstituted pyrenes **6a-d** bearing three alkoxy groups at each phenyl ring show a decreasing order with values of 181 °C (*n*-butyl), 149 °C (*n*-hexyl), 87 °C (*n*-octyl) and 78 °C (*n*-decyl), respectively. This observation can be explained by steric effects of long alkyl chains preventing the efficient molecular packing in the crystalline state of the corresponding pyrene derivatives. The melting points of the 4,5,9,10-tetrasubstituted pyrenes **6e-h** bearing one alkoxy group at each phenyl ring show a decreasing order with values of >330 °C (*n*-butyl), 218 °C (*n*-hexyl), 179 °C (*n*-octyl) and 144 °C (*n*-decyl), respectively.

In order to investigate liquid crystalline behaviour of the 4,5,9,10-tetra(arylethynyl) modified pyrene derivatives, polarized optical microscopy measurements were performed by heating/cooling the samples in a temperature range of 350 – 0°C. Exclusively, pyrene **6d** with three decyloxy chains at each peripheral phenyl rings shows a monotropic phase transition. The mesophase was observed in a narrow temperature range between 44-58 °C (Figure 3) indicating that the presence of an increasing number of extended alkyl chains promotes the liquid crystalline behaviour. The optical texture is characteristic for the appearance of discotic nematic (N_D) mesophase which is typically for planar polyaromatics.

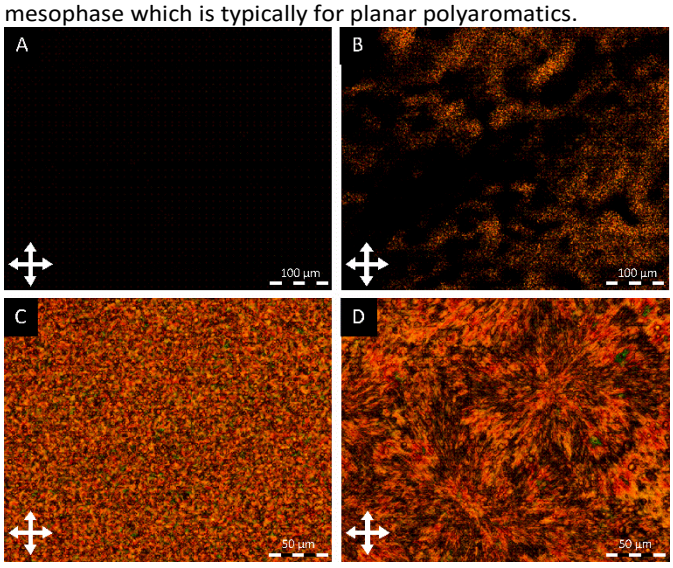

Figure 3. POM images of **6d**, (*A*) at 90 °C, (*B*) cooling to 58 °C, (*C*) at 55 °C at a higher magnification factor, (*D*) cooling to 40 °C. Pictures *B* and *C* show the typical optical textures of a discotic nematic (N_D) mesophase, whereas crystalline domains are observed at 40 °C.

To the best of our knowledge, this is the first example of a 4,5,9,10-functionalized pyrene derivative providing liquid crystalline characteristics which were not prevented by steric effects of the bulky *tert*-butyl groups attached to the pyrene core. Based on these promising results, the investigated polyaromatic pyrene compounds are interesting precursors for the preparation of mesogenic emitter molecules with tuneable photophysical properties and solid-state characteristics.

Conclusions

In conclusion, 4,5,9,10-tetra(arylethynyl)pyrenes bearing hydrophobic alkoxy groups at the periphery of the polyaromatic core have been successfully synthesized through a straightforward SONOGASHIRA coupling approach. Investigations of the photophysical properties in various solvents and in the solid state indicate the presence of aggregation induced excimer pairs which were surprisingly not prevented by bulky *tert*-butyl groups at the pyrene core. The co-planar alignment and characteristic π-π-displaced interactions of adjacent molecules is confirmed by our in deep crystallographic analysis supported by theoretical calculations, indicating that a dense molecular packing is not inhibited by the long alkyl chains or the bulky *tert*-butyl groups. Furthermore, changing the hydrophobicity of the pyrene derivatives by variation of the alkyl ether substitution pattern and the chain length results in tuneable aggregation behaviour and molecular self-assembly of the corresponding pyrene derivatives. These effects are proved by monitoring excimer induced optical characteristics such as quantum yield changes and/or bathochromic shifts of the emission maxima. Pyrene **6d** bearing three decyloxy chains at each phenyl ring shows a transition between the isotropic and discotic nematic (N_D) mesophase in a temperature range of 14 °C. Based on these results, the prepared 4,5,9,10-tetrasubstituted pyrenes are promising polyaromatic emitters with tuneable photophysical and liquid crystalline properties which might find potential applications as OLED materials or organic sensor molecules.

Conflicts of interest

There are no conflicts to declare.

Acknowledgements

We would like to thank the Deutsche Forschungsgemeinschaft (DFG, GI882/2-1) for the financial support.

Notes and references

‡ Crystallographic data for the structure have been deposited with the Cambridge Crystallographic Data Centre (CCDC), 12 Union Road, Cambridge CB21EZ, UK. Copies of the data can be obtained free of charge on quoting the depository numbers CCDC 1895645-1895646.

Synthetic procedures and analytical data of the 4,5,9,10-tetra(arylethynyl) pyrenes **6a-h** and the corresponding precursors are provided in the Supporting Information section.

1 L. Xiao, Z. Chen, B. Qu, J. Luo, S. Kong, Q. Gong و J. Kido, *Adv. Mater.*, 2011, **23**, 926–952.
2 M. Shimizu و T. Hiyama, *Chem. Asian. J.*, 2010, **5**, 1516–1531.
3 B. Y. Guo, G. Yu و Y. Liu, *Adv. Mater*, 2010, **22**, 4427–4447.
4 Y. Tao, C. Yang و J. Qin, *Chem. Soc. Rev.*, 2011, **40**, 2943–2970.
5 M. Zhu و C. Yang, *Chem. Soc. Rev.*, 2013, **42**, 4963–4976.
6 L. Duan, L. Hou, T. Lee, J. Qiao, D. Zhang و G. Dong, *J. Mater. Chem*, 2010, **20**, 6392–6407.
7 J. Jou, S. Kumar, A. Agrawal و T. Li, *J. Mater. Chem. C*, 2015, **3**, 2974–3002.
8 P.-T. Chou و Y. Chi, *Chem. Eur. J.*, 2007, **13**, 380–395.
9 X.-H. Zhu, J. Peng, Y. Cao و J. Roncali, *Chem. Soc. Rev.*, 2011, **40**, 3509–3524.
10 K. Albrecht, K. Matsuoka, K. Fujita و K. Yamamoto, *Angew. Chem, Int. Engl.*, 2015, **54**, 5677–5682.
11 F. Loiseau, S. Campagna, A. Hameurlaine و W. Dehaen, *J. Am. Chem. Soc*, 2005, **127**, 11352–11363.
12 N. D. Mcclenaghan, R. Passalacqua, S. Campagna, B. Verheyde, A. Hameurlaine و W. Dehaen, *J. Am. Chem . Soc.*, 2003, **125**, 5356–5365.
13 G. Deng, Q. Feng, M. Yang, Q. Wang, H. Xu, J. Liu, S. Bo, X. Zhang و Z. Li, *Materials Letters*, 2017, **193**, 112–114.
14 C. Duan, J. Li, C. Han, D. Ding, H. Yang, Y. Wei و H. Xu, *Chem. Mater.*, 2016, **28**, 5667–5679.
15 A. Herrmann, T. Weil, V. Sinigersky, U.-M. Wiesler, T. Vosch, J. Hofkens, F. C. De Schryver و K. Müllen, *Chem. Eur. J.*, 2001, **7**, 4844–4853.
16 S. Bernhardt, M. Kastler, V. Enkelmann, M. Baumgarten و K. Müllen, *Chem. Eur. J.*, 2006, **12**, 6117–6128.
17 Y. Liu, S. Chen, J. W. Y. Lam, F. Mahtab, H. S. Kwok و B. Z. Tang, *J. Mater. Chem*, 2012, **22**, 5184–5189.
18 Z. Zhao, C. Y. K. Chan, S. Chen, C. Deng, J. W. Y. Lam, C. K. W. Jim, Y. Hong, P. Lu, Z. Chang, X. Chen, P. Lu, H. S. Kwok, H. Qiu و B. Tang, *J. Mater. Chem*, 2012, **22**, 4527–4534.
19 C.-H. Chien, L.-R. Kung, C.-H. Wu, C.-F. Shu, S.-Y. Chang و Y. Chi, *J. Mater. Chem*, 2008, **18**, 3461–3466.
20 X. Liu, J. Xu, X. Lu و C. He, *Org. Lett.*, 2005, **7**, 2829–2832.
21 B. R. N. Bera, N. Cumpstey, P. L. Burn و I. D. W. Samuel, *Adv. Funct. Mater.*, 2007, **17**, 1149–1152.
22 G. Schweicher, G. Gbabode, F. Quist, O. Debever, N. Dumont, S. Sergeyev و Y. H. Geerts, *Chem. Mater*, 2009, **21**, 5867–5874.
23 E. J. Foster, R. B. Jones, C. Lavigueur و V. E. Williams, *J. Am. Chem. Soc*, 2006, **128**, 8569–8574.
24 T. Kato, T. Yasuda, Y. Kamikawa و M. Yoshio, *Chem. Commun.*, 2009, 729–739.
25 T. M. Figueira-Duarte و K. Müllen, *Chem. Rev.*, 2011, **111**, 7260–7314.
26 X. Feng, J. Y. Hu, C. Redshaw و T. Yamato, *Chem. Eur. J.*, 2016, **22**, 11898–11916.
27 K. P. Gan, M. Yoshio و T. Kato, *J. Mater. Chem. C*, 2016, **4**, 5073–5080.
28 Y. Sagara و T. Kato, *Nature chemistry*, 2009, **1**, 605–610.
29 Y. Kamikawa و T. Kato, *Langmuir*, 2007, **23**, 274–278.
30 Y. Kamikawa و T. Kato, *Org. Lett.*, 2006, **8**, 2463–2466.
31 J. Fan, L. Ding, Y. Bo و Y. Fang, *ACS Applied Materials and Interfaces*, 2015, **7**, 22487–22496.
32 C. Wang, C. Wu, Y. Chen, Y. Song, W. Tan و C. J. Yang, *Current Organic Chemistry*, 2011, **15**, 465–476.
33 J. Fan, D. Zheng, X. Huang, L. Ding, Y. Xin و Y. Fang, *Sensors and Actuators, B: Chemical*, 2018, **263**, 336–346.
34 D. Kraskouskaya, M. Bancerz, H. S. Soor, J. E. Gardiner و P. T. Gunning, *Journal of the American Chemical Society*, 2014, **136**, 1234–1237.
35 L. Jia, L. Xu, Z. Wang, J. Xu و J. Ji, *Chinese Journal of Chemistry*, 2014, **32**, 85–90.
36 A. Kapf و M. Albrecht, *Journal of Materials Chemistry B*, 2018, **6**, 6599–6606.
37 H. Y. Oh, C. Lee و S. Lee, *Organic Electronics: physics, materials, applications*, 2009, **10**, 163–169.
38 X. Gong, X. Xie, N. Chen, C. Zheng, J. Zhu, R. Chen, W. Huang و D. Gao, *Chin. J. Chem.*, 2015, **33**, 967–973.
39 J. N. Moorthy, P. Natarajan, P. Venkatakrishnan, D. F. Huang و T. J. Chow, *Org. Lett.*, 2007, **9**, 5215–5218.
40 T. M. Figueira-Duarte, S. C. Simon, M. Wagner, S. I. Druzhinin, K. A. Zachariasse و K. Müllen, *Angewandte Chemie - International Edition*, 2008, **47**, 10175–10178.
41 J. Lee, H. Jung, H. Shin, J. Kim, D. Yokoyama, H. Nishimura, A. Wakamiya و J. Park, *J. Mater. Chem. C*, 2016, **4**, 2784–2792.
42 J. Yang, L. Li, Y. Yu, Z. Ren, Q. Peng, S. Ye, Q. Li و Z. Li, *Mater. Chem. Front.*, 2017, **1**, 91–99.
43 T. Hirose, T. Yumoto, K. Matsumoto, S. Mitsushio, O. Kawakami و M. Yasutake, *Mol. Cryst. Liq. Cryst*, 2010, **524**, 68–101.
44 C. Krause و A. Schönhals, *J. Phys. Chem. C*, 2013, **117**, 19712–19720.
45 F. Xu, T. Nishida, K. Shinohara, L. Peng, M. Takezaki, T. Kamada, H. Akashi, H. Nakamura, K. Sugiyama, K. Ohta, A. Orita و J. Otera, *Organometallics*, 2017, **36**, 556–563.
46 S. Diring, F. Camerel, B. Donnio, T. Dintzer, S. Toffanin, R. Capelli, M. Muccini و R. Ziessel, *J. Am. Chem . Soc.*, 2009, **131**, 18177–18185.
47 T. Hirose, Y. Shibano, Y. Miyazaki, N. Sogoshi, S. Nakabayashi و M. Yasutake, *Mol. Cryst. Liq. Cryst.*, 2011, **534**, 81–92.
48 H. Anetai, Y. Wada, T. Takeda, N. Hoshino, S. Yamamoto, M. Mitsuishi, T. Takenobu و T. Akutagawa, *J. Phys. Chem. Lett.*, 2015, **6**, 1813–1818.
49 Y. Sagara و T. Kato, *Angew. Chem, Int. Engl.*, 2008, **47**, 5175–5178.
50 B. V. De Halleux, J. Calbert, P. Brocorens, J. Cornil, J. Declercq, J. Brødas و Y. Geerts, *Adv. Funct. Mater.*, 2004, **14**, 649–659.
51 J. Oh, Y. O. Lee, T. H. Kim, K. C. Ko, J. Y. Lee, H. Kim و J. S. Kim, *Angew. Chem, Int. Ed.*, 2009, **48**, 2522–2524.
52 Y. O. Lee, T. Pradhan, S. Yoo, T. H. Kim, J. Kim و J. S. Kim, *J. Org. Chem.*, 2012, **77**, 11007–11013.
53 A. Hayer, V. de Halleux, A. Köhler, A. El-Garoughy, E. W. Meijer, J. Barbera, J. Tant, J. Levin, M. Lehmann, J. Gierschner, J. Cornil و Y. H. Geerts, *J. Phys. Chem. B*, 2006, **110**, 7653–7659.

54 K. Fujimoto, H. Shimizu, M. Furusyo, S. Akiyama و M. Ishida, *Tetrahedron*, 2009, **65**, 9357–9361.

55 G. Venkataramana و S. Sankararaman, *Eur. J. Org. Chem.*, 2005, 4162–4166.

56 A. G. Crawford, Z. Liu, I. A. I. Mkhalid, M. H. Thibault, N. Schwarz, G. Alcaraz, A. Steffen, J. C. Collings, A. S. Batsanov, J. A. K. Howard و T. B. Marder, *Chem. Eur. J.*, 2012, **18**, 5022–5035.

57 A. G. Crawford, A. D. Dwyer, Z. Liu, A. Ste, A. Beeby, L.-O. Palsson, D. J. Tozer و T. B. Marder, *J. Am. Chem. Soc.*, 2011, **133**, 13349–13362.

58 S. Kato, H. Kano, K. Irisawa, N. Yoshikawa و R. Yamamoto, *Org. Lett.*, 2018, **20**, 7530–7534.

59 S. Setia و S. Kumar, *ChemistrySelect*, 2016, **5**, 880–885.

60 P. Y. Gu, Z. Wang, G. Liu, H. Yao, Z. Wang, Y. Li, J. Zhu, S. Li و Q. Zhang, *Chem. Mater.*, 2017, **29**, 4172–4175.

61 Y. Miura و E. Yamano, *J. Org. Chem.*, 1995, **60**, 1070–1073.

62 J. Y. Hu, M. Era, M. R. J. Elsegood و T. Yamato, *Eur. J. Org. Chem.*, 2010, 72–79.

63 J.-Y. Hu, X.-L. Ni, X. Feng, M. Era, M. R. J. Elsegood, S. J. Teat و T. Yamato, *Org. Biomol. Chem.*, 2012, **10**, 2255.

64 W. Zhao و F. N. Castellano, *J. Phys. Chem. A*, 2006, **110**, 11440–11445.

65 F. Winnik, *Chem. Rev.*, 1993, **93**, 587–614.